JACS
JOURNAL OF THE AMERICAN CHEMICAL SOCIETY
Article
pubs.acs.org/JACS

Mass Action at the Single-Molecule Level

Min Ju Shon and Adam E. Cohen*

Department of Chemistry and Chemical Biology and Department of Physics, Harvard University, Cambridge, Massachusetts 02138, United States

Supporting Information

ABSTRACT: We developed a system to reversibly encapsulate small numbers of molecules in an array of nanofabricated "dimples". This system enables highly parallel, long-term, and attachment-free studies of molecular dynamics via single-molecule fluorescence. In studies of bimolecular reactions of small numbers of confined molecules, we see phenomena that, while expected from basic statistical mechanics, are not observed in bulk chemistry. Statistical fluctuations in the occupancy of sealed reaction chambers lead to steady-state fluctuations in reaction equilibria and rates. These phenomena are likely to be important whenever reactions happen in confined geometries.

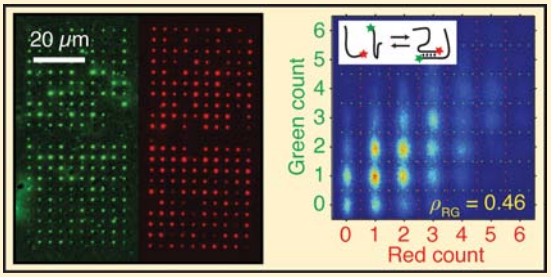

INTRODUCTION

Many biochemical reactions take place within the confines of membrane-bound structures. When small numbers of molecules are present, stochastic fluctuations in molecule number play a significant role in determining reaction outcomes.[1−4] The importance of these fluctuations increases as the order of the reaction increases and as the absolute number of molecules decreases. We asked: how do statistical fluctuations in occupancy affect the thermodynamics and kinetics of reactions in confinement?

We developed a "Dimple Machine" to study reactions in confinement via single-molecule fluorescence (Figure 1). The device enables highly parallel, long-term, and attachment-free studies of single molecules or small numbers of molecules confined in nanofabricated chambers. Confinement has previously been used in single-molecule studies, but under conditions where the confined region was large compared to the optical wavelength or where the confinement was in self-assembled structures lacking precisely defined sizes and locations.[5−13] Here we achieved sufficiently tight confinement that (a) the radius of confinement was small compared to the mean separation of reactant molecules in bulk solution and (b) the radius of confinement was small enough that all possible pairwise intermolecular collisions occurred on an experimentally accessible time scale. This qualitatively new regime led to several apparent deviations from the law of mass action, which are reconciled by a statistical description of reactivity in confinement.

The heart of the Dimple Machine is a fused silica coverslip containing multiple arrays of nanofabricated circular depressions, or "dimples", with diameters ranging from 70 nm to 1.3 μm and a depth of 200 nm (Figure 1c,d). The dimples were bathed in a solution of fluorescent molecules, and a pneumatically actuated polymer lid reversibly sealed the dimples (Figure 1a). The lid trapped in each dimple a minute volume of solution and a small number of fluorescent molecules. The array of trapped molecules was imaged on a fluorescence microscope (Figure 1b,e).[14,15] After imaging, the lid was opened, molecules in the dimples interchanged with fresh ones from the bulk, and the process was repeated an arbitrary number of times.

We used a Dimple Machine to study the fundamental chemistry of a simple bimolecular reaction in confinement. Two strands of single-stranded DNA (ssDNA) labeled with fluorescent dyes were trapped together in the dimples, and their hybridization was monitored by colocalization and by fluorescence resonance energy transfer (FRET). In each trapping cycle there were small-number fluctuations in the number of DNA molecules in each dimple. We found that confinement rectified these fluctuations, leading to dimple-to-dimple fluctuations in equilibria and rate constants. The observations are quantitatively explained by a modification to the law of mass action to incorporate local concentration fluctuations.

Dimple Machine technology provides a possible resolution to many challenges associated with single-molecule measurements in solution.[13] Molecules in free solution are typically observed for fleeting moments due to diffusion, while surface tethering may disrupt molecular function. Feedback systems[6] or spatial confinement[5,7−12] provide an approach to keep molecules within an observation volume while permitting unconstrained motion on the molecular scale. Confinement in 2-D sheets[7] or 1-D channels[5] does not completely suppress Brownian motion, while confinement in vesicles[8−10] leaves molecules randomly distributed and does not provide precise control over the confinement volume or a means of replenishing the molecules after photobleaching. Confinement in etched optical fiber bundles has been used to study single-molecule dynamics,[11] but the requirement that the lateral dimensions be comparable to

Received: June 26, 2012
Published: August 13, 2012

   dx.doi.org/10.1021/ja3062425 | J. Am. Chem. Soc. 2012, 134, 14618−14623

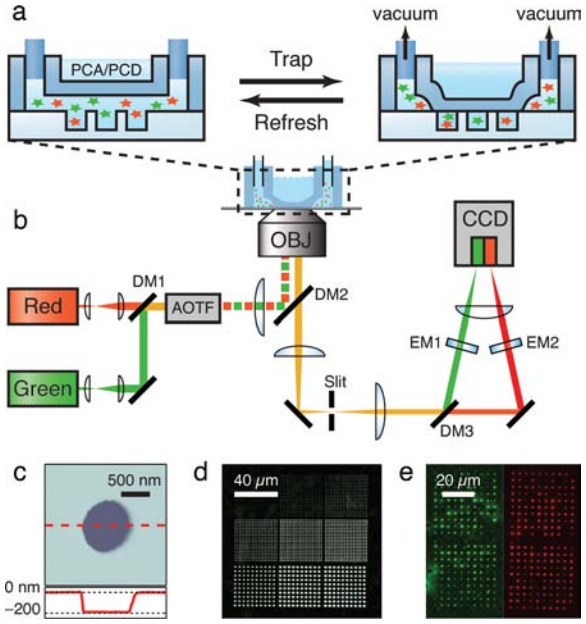

Figure 1. Experimental scheme for the Dimple Machine. (a) Trapping and refreshing cycle with actuation of the lid. A buffer solution on top of the semipermeable lid prevented sealed dimples from drying out and deoxygenated the environment to minimize photobleaching. PCA = protocatechuic acid; PCD = protocatechuate-3,4-dioxygenase. (b) Optical setup for fluorescence imaging in two colors. An inverted microscope is equipped with alternating red and green laser excitation and a dual-view camera. OBJ = objective; DM = dichroic mirror; AOTF = acousto-optic tunable filter; EM = emission filter; CCD = charge-coupled device. (c) Atomic force microscope image of a dimple with a nominal radius of 450 nm. (d) Dark-field microscope image of a dimple array containing 900 dimples of various sizes. (e) FRET imaging of DNA molecules trapped in a dimple array with (left) donor and (right) acceptor fluorescence, both with green excitation of the donor. The original image was acquired by a dual-view CCD and background-subtracted and pseudocolored for visualization.

the optical wavelength leads to confinement volumes significantly larger than those described here. The Dimple Machine reversibly confines molecules to well-defined volumes at well-defined locations. The device uses a small sample (usually less than a picomole), acquires a large data set automatically, and can be reused indefinitely.

RESULTS

Dimple Machine Confines Molecules Reproducibly and Free of Surface Artifact. Each array in the Dimple Machine contained 900 wells, arranged in a square lattice with spacing 4 μm (Figure 1e). The volume per dimple ranged from 8×10^{-19} to 2.6×10^{-16} L, corresponding to concentrations at unimolecular occupancy between 2.2 μM and 6.3 nM (Figure S1, Supporting Information). The lid was made of a polydimethylsiloxane (PDMS) membrane (Figures S2 and S3, Supporting Information). The operation of the device was fully automated so that the trap−measure−refresh cycle could be repeated an arbitrary number of times (Section S1, Supporting Information).

We faced a number of technical challenges associated with background autofluorescence from the fused silica and PDMS, suppressing photobleaching of fluorescent dyes, preventing sticking of molecules inside the dimples, preventing leakage of molecules out of the dimples, diffusion of water into the PDMS lid leading to drying of the dimples, reproducible sealing of the dimples, and avoidance of air bubbles in the microfluidic sample channel. Our solutions to these challenges are presented in the Supporting Information (Section S2). In particular, photobleaching was drastically suppressed by integrating three levels of deoxygenation: (a) enzymatic oxygen scavenging in microchannels, (b) remote deoxygenation from across the lid membrane, and (c) operation of the device under a nitrogen atmosphere (Figure S4, Supporting Information).

A typical Dimple Machine trapping run proceeded as follows: 40 μL of sample at 2−100 nM was injected into the device, pneumatic actuation caused the lid to close onto the dimples, sealing them hermetically within 2 min, N_1 = 200 dimples containing molecules were imaged for 1−5 min, the lid was opened and the contents of the dimples were exchanged with the bulk for 1 s, and the cycle was repeated for N_2 = 200 times, at a rate of ∼10 cycles/h. This experiment generated a data set consisting of $N_1 \times N_2$ = 40 000 dimples.

Occupancy of Dimples Fluctuates Statistically. To validate the device, we ran several tests with 30-mer ssDNA oligos labeled with Cy5. The occupancy of dimples, N, was measured by the fluorescence intensity (Figure 2). First, the

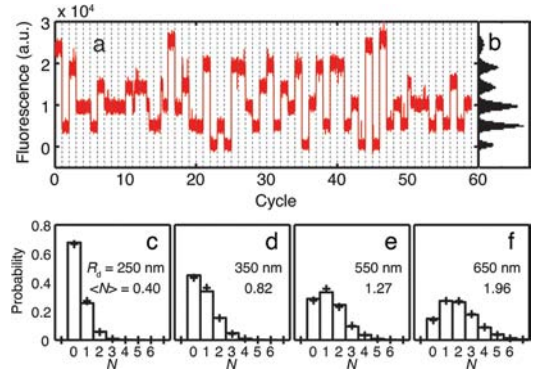

Figure 2. Occupancy of dimples. (a) Fluorescence time traces from one dimple (R_d = 650 nm) concatenated over 60 trapping cycles. Cycles lasted 1 min and were spaced by 5 min. The dashed lines break the trace into individual cycles. (b) Histogram of fluorescence intensity measured in (a). The spacing between the peaks corresponds to the unit fluorescence from a single fluorophore. (c−f) Occupancy distribution of the dimples. The sample concentration was 8.4 nM for all. R_d = radius of the dimples; $\langle N \rangle$ = mean occupancy.

unit fluorescence of a single dye was assessed from the spacing of evenly spaced peaks in the fluorescence intensity histogram (Figure 2b). The occupancy was obtained by dividing the total fluorescence from a dimple by this unit and rounding to the nearest integer. The well-resolved peaks in the intensity histogram (Figure 2b) indicate that this procedure is robust. This calibration was performed separately for each dimple to correct for small variations in laser illumination intensity and collection efficiency (Figure S5, Supporting Information). The maximum countable occupancy was ∼15 molecules/dimple (Figure S5).

The occupancy varied between dimples within a trapping cycle, and within each dimple over multiple trapping cycles, but not within a single dimple during a single trapping cycle (except for slight photobleaching at 3%/min), thus establishing that molecules were completely sealed within the dimples. There were negligible differences in mean occupancy between dimples of the same nominal size, thus ruling out static heterogeneity

dx.doi.org/10.1021/ja3062425 | J. Am. Chem. Soc. 2012, 134, 14618−14623

due to variations in nanofabrication. There were no long-term drifts in the mean dimple occupancy over many trapping cycles, thus ruling out evaporation or adsorption as causes of long-term instability. Finally, the occupancy of each dimple was uncorrelated between measurement cycles, thus ruling out artifacts from sticking of molecules to the walls of the dimple or the PDMS lid (Figure S6, Supporting Information).

Dimple occupancy, N, was Poisson distributed with mean $\langle N \rangle \approx cV_d$, where c is the concentration in bulk and V_d is the volume of a dimple (Figure 2c–f). For each experiment we adjusted c to achieve a desired $\langle N \rangle$. These results established that the Dimple Machine reversibly encapsulated molecules in well-defined volumes, without strong surface interactions.

Correlation in Occupancy Measures Molecular Affinity. Consider the reaction

$$R + G \rightleftarrows RG$$

where R and G are any two species, each labeled with a single red or green dye. The fraction of molecules in the dimerized RG state is governed by the dissociation constant, K_d. Suppose molecules from a solution of R and G are trapped in the dimples and the total numbers of red and green dyes ($N_R^{(T)} = N_R + N_{RG}$ and $N_G^{(T)} = N_G + N_{RG}$) are counted in each dimple. If R and G do not interact, then the distributions of $N_R^{(T)}$ and $N_G^{(T)}$ will be statistically independent (Figure 3a). If R and G are fused or interact very strongly, then the distributions of $N_R^{(T)}$ and $N_G^{(T)}$ will be highly correlated (Figure 3b). For an intermediate-strength interaction, R and G will colocalize more often than one would expect from chance, but not perfectly. Mathematically, the probability distribution of joint occupancy, $P(N_R^{(T)},N_G^{(T)})$, is described by a correlated bivariate Poisson distribution (Section S3, Supporting Information), whose parameters are related to the concentrations [R], [G], and [RG] in bulk. Fitting this model to the measured distribution of occupancy gives an estimate for K_d (Figure S7, Supporting Information).

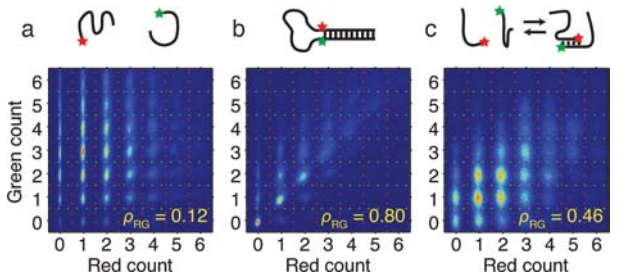

Figure 3. Molecular affinity probed by joint occupancy: (top) cartoon of DNA interactions with (a) no, (b) strong, and (c) weak affinity; (bottom) experimental red–green (R-G) histograms of joint occupancy. The procedure for converting raw movies into R-G histograms is described in Section S1 and Figure S7 (Supporting Information).

Note that the determination of K_d via correlated occupancy does not rely on FRET. This procedure is expected to work well for dimple occupancies small enough that the occupancy can be counted. We readily count >10 fluorophores of each color, corresponding to molecular concentrations up to ~10 μM. This concentration sets the upper bound on K_d that can be measured by this technique, which is much higher than the maximum K_d that can be measured by fluorescence cross-correlation spectroscopy.[16]

We tested the correlated occupancy method in three DNA constructs. In the first, we mixed two noncomplementary ssDNA strands, one labeled with Cy3 and the other with Cy5. The 2D histogram of red and green fluorescence (R-G histogram, Figure 3a, bottom) showed peaks around integer occupancy of each dimple. By eye, the red and green distributions look independent. We tested for independence by comparison to the theoretically predicted joint probability distribution (Section S3, Supporting Information).

In the second test, we made a hairpin construct doubly labeled with one red dye (Alexa 647) and one green dye (Cy3B). Due to efficient FRET from the green to the red dye, the number of green fluorophores per dimple was estimated by exciting with green light and summing the fluorescence from the red and green channels. Here the joint distribution was strongly peaked along the diagonal, $N_R^{(T)} = N_G^{(T)}$, as one would expect (Figure 3b). We attribute the weak off-diagonal peaks to imperfect labeling. Indeed, this measurement lets us estimate the labeling efficiencies, which were 89% with Alexa 647 and 72% with Cy3B.

The third sample contained two ssDNA oligos of length 30 bp, with an 8 bp complementary region at their 5′-termini (Figure 3c). The oligos were labeled with Cy3 and Cy5, respectively, on their 5′-ends. The dimerized state showed efficient FRET. As in the case of the hairpin, we estimated the number of Cy3 molecules by summing the red and green emission under green excitation. As expected from the weak association through base pairing, the correlation in the joint occupancy was intermediate between the two extremes. We quantified the red–green correlation by calculating correlation coefficients (ρ_{RG}) (Figure 3 and Table S4 (Supporting Information)), and from this we calculated K_d = 63 ± 12 nM. This measurement agreed well with a bulk titration in a fluorimeter (57 ± 12 nM, Figure S8 (Supporting Information)) and with a theoretical prediction (44–110 nM at 17–20 °C).[17]

We next studied the hybridization reaction in detail to determine the effect of fluctuations in occupancy on this reaction.

Reversible Bimolecular Reaction: DNA Hybridization. Alternating laser fluorescence measurements[14] determined the complete time-dependent reaction state within each dimple: (a) red emission under red excitation indicated the total number of red dyes ($N_R + N_{RG}$), (b) red emission under green excitation indicated the number of dye pairs capable of undergoing FRET (N_{RG}), and (c) green emission under green excitation indicated the number of green dyes not quenched by a red acceptor (N_G). We observed that the reaction thermodynamics and kinetics varied with dimple occupancy and size, even for identical bulk concentrations of reactants.

More Products in Highly Occupied, Small Dimples. We examined the effect of occupancy on reaction thermodynamics. Fluorescence time traces were first categorized by $(N_R^{(T)},N_G^{(T)})$ with the integers $N_R^{(T)}$ and $N_G^{(T)}$ representing the total numbers of red and green strands, irrespective of hybridization state (Figure 4a). For each occupancy, we then studied the distribution of dimers, $P(N_{RG})$. We excited with green light and made a 2D histogram of green and red emission, indicating donor and acceptor fluorescence (D-A histogram). Parts b–e of Figure 4 show these histograms for the cases $N_R^{(T)} = N_G^{(T)}$, though the analysis is not restricted to symmetric occupancy. The D-A histogram clearly resolved multiple states of reaction corresponding to distinct numbers of

dx.doi.org/10.1021/ja3062425 | J. Am. Chem. Soc. 2012, 134, 14618–14623

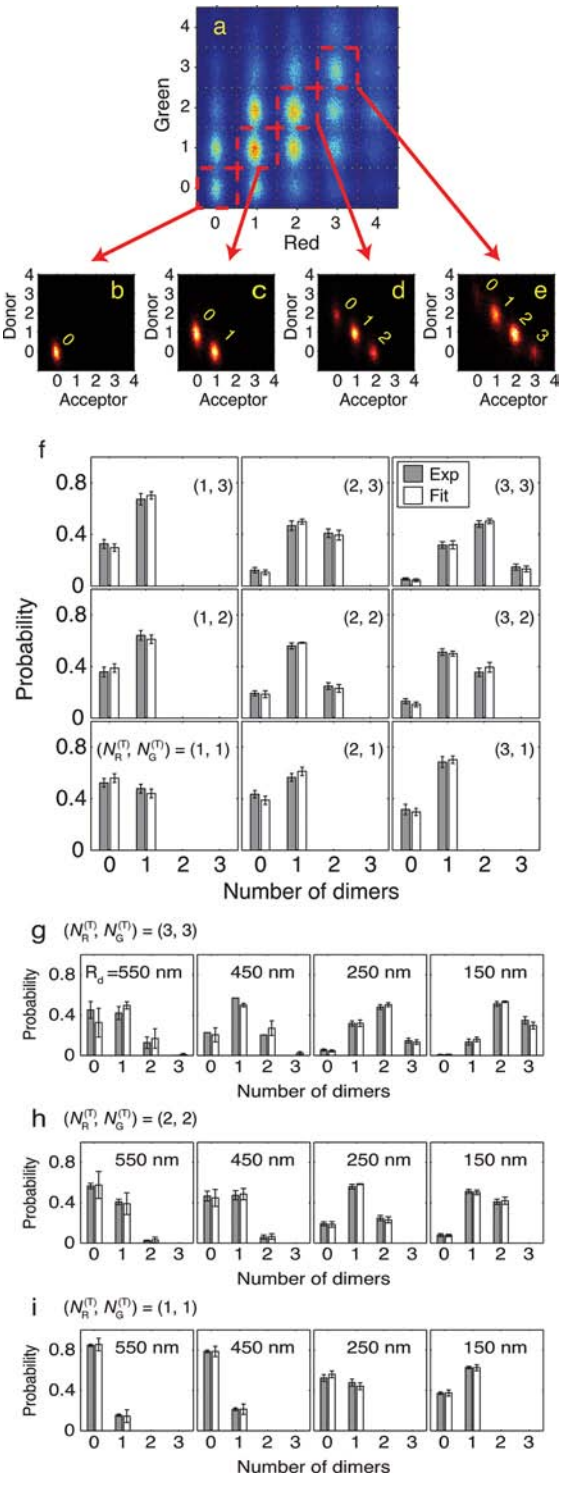

Figure 4. Thermodynamics of hybridization in confinement. (a) Red–green histogram showing correlated occupancy of dimples, as expected from a weak association of R and G in bulk. (b–e) Donor–acceptor histogram indicating probability distribution of RG pairs, $P(N_{RG})$, for different dimple occupancies, $(N_R^{(T)},N_G^{(T)})$: (b) $(N_R^{(T)},N_G^{(T)}) = (0, 0)$; (c) $(N_R^{(T)},N_G^{(T)}) = (1, 1)$; (d) $(N_R^{(T)},N_G^{(T)}) = (2, 2)$; (e) $(N_R^{(T)},N_G^{(T)}) = (3, 3)$. (f) Distribution of dimers as a function of joint occupancy: Exp, experimental; Fit: fit to Markovian reaction model (Section S5, Supporting Information). (g–i) Distribution of dimers as a function of dimple size at the given joint occupancy.

dimers. The maximum number of dimers varied with dimple occupancy according to $N_{RG}^{max} = \min(N_R^{(T)},N_G^{(T)})$ as expected.

The relative intensities of the peaks in the D-A histogram gave the distribution $P(N_{RG})$. Figure 4f shows the probability distribution $P(N_{RG})$ for dimples of the same size (R_d = 250 nm), but different occupancy. The reaction equilibrium shifted toward the dimer at higher occupancy (compare $(N_R^{(T)},N_G^{(T)})$ = (1, 1), (1, 2), and (1, 3) or $(N_R^{(T)},N_G^{(T)})$ = (2, 2) and (2, 3)). Note that these data were all taken at the same nominal bulk ssDNA concentration, 30 nM. The variations in equilibrium were purely due to small-number fluctuations in occupancy. Other sizes of dimples (R_d = 150, 450, and 550 nm) showed the same trend.

The shift in equilibrium is easily explained if one invokes the local concentration of each species in the dimple, rather than the bulk concentration. We define the local concentration (c_{local}) of each species as

$$c_{local} = \frac{N}{N_A V_d} \quad (1)$$

where N is the number of molecules, N_A is Avogadro's number, and V_d is the volume of a dimple. The mean number of dimers per dimple is then given by the usual equilibrium expression.

Within each dimple we obtain the distribution $P(N_{RG})$, not just its mean. This distribution can be simulated by modeling the reaction in the dimple as a finite-state Markov process:

$$\dot{\mathbf{P}} = \mathbf{MP} \quad (2)$$

where $\mathbf{P} = P(N_{RG})$ describes the state of the system and $\mathbf{M}$ is a kinetic matrix. The dimension of $\mathbf{P}$ is $N_{RG}^{max} + 1$. The form of $\mathbf{M}$ depends on dimple size and occupancy $(N_R^{(T)},N_G^{(T)})$. Details of the construction of $\mathbf{M}$ are given in Section S5 (Supporting Information).

Solving eq 2 for $\dot{\mathbf{P}} = 0$ yields equilibrium distributions $P(N_{RG})$ in quantitative agreement with experiment. This model has only a single fitting parameter, K_d. Applying a global fit to all occupancies yielded $K_d = 56 \pm 4$ nM ("Fit" of Figure 4f). This value agreed with the previous measurements of K_d on this sample (Table 1). The fact that a single value K_d of can describe the equilibrium for all occupancies implies that the occupancy did not affect the free energies of molecules but tipped the balance of reaction by changing c_{local}.

To see the effect of dimple size on equilibrium, the dimer distributions in dimples of different sizes were compared at the same occupancy (Figure 4g–i). For a given occupancy, smaller dimples had higher dimer concentration. This trend can be explained again by the change in c_{local}, with smaller dimples having higher c_{local} values when occupied, and thus an equilibrium shifted toward the product.

The K_d's for all dimple sizes were comparable (Table 1). This result confirms that the apparent shift in equilibrium is due to rectification of small-number fluctuations, not a change in the intrinsic nature of the hybridization. A relatively large K_d in the smallest dimples (R_d = 150 nm) might be due to surface interactions reducing the effective concentration.

Faster Reaction in Highly Occupied, Small Dimples. We next examined the effects of confinement on reaction kinetics (Figure 5). The fluorescence traces showed clear stepwise changes in FRET corresponding to single association and dissociation events (Figure 5a). The intensity of acceptor fluorescence was a direct indicator of the number of dimers. We studied the autocorrelation of acceptor fluorescence:

$$C_{AA}^{(2)}(\tau) = \langle \delta A(t)\delta A(t+\tau)\rangle_t \quad (3)$$

dx.doi.org/10.1021/ja3062425 | J. Am. Chem. Soc. 2012, 134, 14618–14623

Table 1. Dissociation Constant (K_d) and Rate Constants (k_{on} and k_{off}) for DNA Hybridization in Dimples

		R_d (nm)			
	bulk	550	450	250	150
K_d (nM)	63 ± 12,[a] 57 ± 12[b]	54 ± 3	51 ± 4	56 ± 4	74 ± 4
k_{on} (10^6 M^{-1} s^{-1})		0.77 ± 0.07	1.09 ± 0.09	1.18 ± 0.07	1.27 ± 0.04
k_{off} (10^{-2} s^{-1})		6.88 ± 0.06	5.96 ± 0.07	6.15 ± 0.08	5.70 ± 0.11

[a]Measured from the correlated occupancy on dimples with R_d = 250 nm (Figure 3 and Section S3 (Supporting Information). [b]Measured in a fluorimeter (Figure S8 and Section S4 (Supporting Information)).

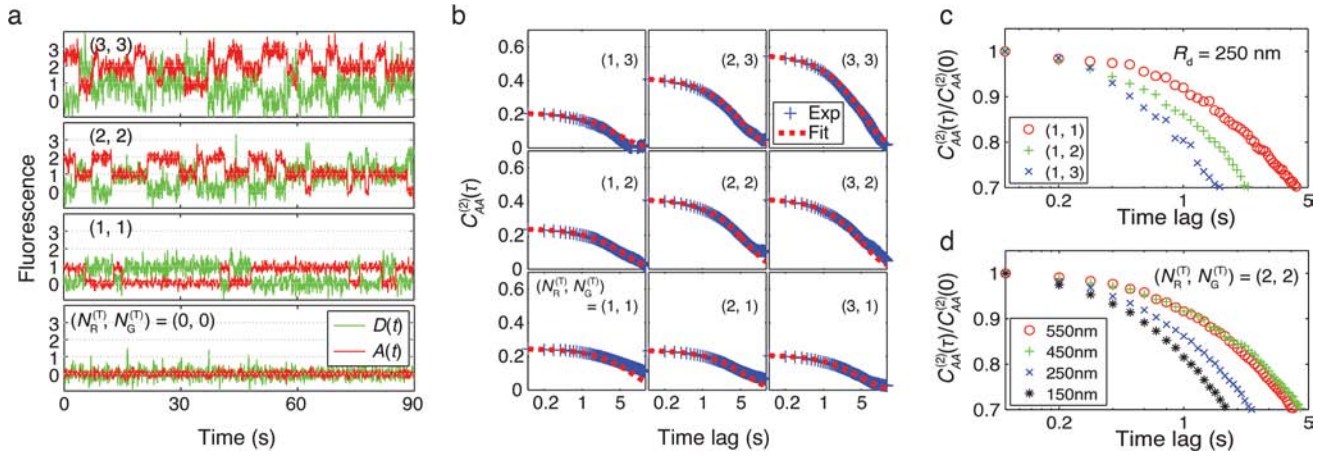

Figure 5. Kinetics of hybridization in confinement: (a)fluorescence time traces monitoring hybridization in dimples with different occupancies; (b) autocorrelation of acceptor fluorescence as a function of occupancy; (c) effect of occupancy on the rates of reaction; (d) effect of dimple size on the rates of reaction. The autocorrelations in (c) and (d) are normalized to unity at zero lag.

where $\delta A(t) = A(t) - \langle A(t)\rangle_t$ is the deviation of acceptor fluorescence at time t from average. The autocorrelation function was different for different dimple occupancies and dimple sizes (Figure 5b–d).

We used the kinetic model of eq 3 to simulate these autocorrelation functions as follows. Integration of eq 2 yields

$$\mathbf{P}(t) = \mathbf{G}(t|t_0)\mathbf{P}(t_0) \tag{4}$$

where $\mathbf{G}(t|t_0) = \exp[\mathbf{M}(t - t_0)]$. The autocorrelation function is then

$$C_{AA}^{(2)}(\tau) = \left[\sum_{N_i,N_f=0}^{N_{RG}^{max}} N_f G(\tau|0) N_i \mathbf{P}_{eq}(N_i)\right] - \langle N_{RG}\rangle^2 \tag{5}$$

where $\mathbf{P}_{eq}$ is the equilibrium probability distribution. This model quantitatively reproduces the amplitude and time scale of the measured autocorrelation, as a function of both dimple occupancy and size.

We performed a global fit of eq 5 to the autocorrelation decays at different occupancies (Section S5, Supporting Information) and obtained values for the rate constants, k_{on} and k_{off}, that were consistent with all the data (Table 1).

The autocorrelation decayed more quickly for smaller dimples or higher occupancy. Both effects arise from the increased c_{local} under these conditions, and thus an increased association rate. The dissociation rate, k_{off}, was independent of dimple size or occupancy.

DISCUSSION

Confinement in nanoscale dimples rectifies statistical fluctuations in concentration that arise and dissipate spontaneously in the bulk solution. Correlated colocalization of two species provides a quantitative measure of association in bulk. When the dimple volume is smaller than the mean volume per molecule in bulk, then single occupancy leads to an effectively higher concentration than in the bulk. Equilibria and reaction rates vary from dimple to dimple, purely due to stochastic fluctuations in occupancy.

An interesting subtlety of this experiment is that if one averages the quantity $\langle N_{RG}\rangle_t/(N_R N_G)$ over all dimples containing at least one red and one green molecule, the equilibrium is shifted in favor of dimers, in comparison to the equilibrium in bulk. This apparent bias occurred because we are calculating the equilibrium conditional on the dimples being occupied, and occupancy by even one molecule of R and one of G led to higher concentrations than those in bulk. To reproduce the bulk ratios of [R], [G], and [RG], one would need to calculate the averages $\langle N_R\rangle$, $\langle N_G\rangle$, and $\langle N_{RG}\rangle$ over all occupancies, *including* empty dimples, prior to evaluating the equilibrium expression. Similarly, the apparent association rates in the dimples were higher than in the bulk, again because those dimples which had at least one of each reactant were at higher concentration than the bulk.

The confinement effects reported here are likely to be significant whenever molecules are confined to nanoscale volumes. Such scenarios commonly occur in vesicles and organelles in eukaryotic cells,[2] in emulsions,[3] and in micro-/nanoreactors.[4] While we focused on a bimolecular reaction, confinement effects will be more pronounced for higher-order reactions, particularly for autocatalytic processes.

The Dimple Machine enables several new kinds of single-molecule experiments. Due to the deeply subwavelength confinement, single-molecule experiments can be performed with high signal-to-noise ratio at high concentrations of reactants. Only the Dimple Machine and small vesicles provide tight enough confinement to observe individual bimolecular

dx.doi.org/10.1021/ja3062425 | J. Am. Chem. Soc. 2012, 134, 14618–14623

association events at the single-molecule level. Zero-mode waveguides also allow single-molecule experiments at high concentrations,[18] but free diffusion out of the waveguide limits observations of untethered molecules to microseconds.

A particularly intriguing application of the Dimple Machine is toward studying weakly interacting complexes. Weak interactions are difficult to quantify because complexes dissociate during most purification protocols. If the interacting species can be fluorescently labeled, then the Dimple Machine enables quantification of the interaction without purification.

Another possible application of the Dimple Machine is toward studying cooperative interactions. In a multimeric complex, there may be a distribution of association states. Description by a single Hill coefficient may miss important features of this distribution. Through fluorescence counting, the Dimple machine enables one to measure directly the underlying distribution of stoichiometries.

■ ASSOCIATED CONTENT

Ⓢ Supporting Information

Figures, tables, and text giving detailed experimental procedures for device construction, measurement, and data analysis, proof-of-principle measurements and optimization of the device, compositions of samples and buffers, measurements of K_d, and the calculations applied in the study. This material is available free of charge via the Internet at http://pubs.acs.org.

■ AUTHOR INFORMATION

Corresponding Author

*E-mail: cohen@chemistry.harvard.edu.

Notes

The authors declare no competing financial interest.

■ ACKNOWLEDGMENTS

This project was supported in part by NSF grant CHE-0910824 and by the Harvard Materials Research Science and Engineering Center (MRSEC) under grant DMR-0820484. Fabrication was performed at the Harvard Faculty of Arts and Sciences (FAS) Center for Nanoscale Systems, a member of the National Nanotechnology Infrastructure Network, supported by NSF award ECS-0335765. Additional support was provided by the Dreyfus Foundation and the Sloan Foundation.

■ REFERENCES

(1) (a) Rothenberger, G.; Grätzel, M. *Chem. Phys. Lett.* **1989**, *154*, 165−171. (b) Polak, M.; Rubinovich, L. *Nano Lett.* **2008**, *8*, 3543−3547.

(2) Holcman, D.; Schuss, Z. *J. Chem. Phys.* **2005**, *122*, 114710−114715.

(3) Landfester, K. *Annu. Rev. Mater. Res.* **2006**, *36*, 231−279.

(4) (a) Barzykin, A. V.; Seki, K.; Tachiya, M. *Adv. Colloid Interface Sci.* **2001**, *89*−*90*, 47−140. (b) Vriezema, D. M.; Comellas Aragonès, M.; Elemans, J. A. A. W.; Cornelissen, J. J. L. M.; Rowan, A. E.; Nolte, R. J. M. *Chem. Rev.* **2005**, *105*, 1445−1490. (c) Sawada, T.; Yoshizawa, M.; Sato, S.; Fujita, M. *Nat. Chem.* **2009**, *1*, 53−56.

(5) (a) Lyon, W. A.; Nie, S. *Anal. Chem.* **1997**, *69*, 3400−3405. (b) Foquet, M.; Korlach, J.; Zipfel, W. R.; Webb, W. W.; Craighead, H. G. *Anal. Chem.* **2004**, *76*, 1618−1626. (c) Kamagata, K.; Kawaguchi, T.; Iwahashi, Y.; Baba, A.; Fujimoto, K.; Komatsuzaki, T.; Sambongi, Y.; Goto, Y.; Takahashi, S. *J. Am. Chem. Soc.* **2012**, *134*, 11525−11532.

(6) (a) Cohen, A. E.; Moerner, W. E. *Appl. Phys. Lett.* **2005**, *86*, 93103−93109. (b) Goldsmith, R. H.; E., M. *Nat. Chem.* **2010**, *2*, 179−186. (c) Fields, A. P.; Cohen, A. E. *Proc. Natl. Acad. Sci. U.S.A.* **2011**, *108*, 8937−8942.

(7) Leslie, S. R.; Fields, A. P.; Cohen, A. E. *Anal. Chem.* **2010**, *82*, 6224−6229.

(8) (a) Boukobza, E.; Sonnenfeld, A.; Haran, G. *J. Phys. Chem. B* **2001**, *105*, 12165−12170. (b) Okumus, B.; Arslan, S.; Fengler, S. M.; Myong, S.; Ha, T. *J. Am. Chem. Soc.* **2009**, *131*, 14844−14849. (c) Chiu, D. T.; Lorenz, R. M.; Jeffries, G. D. M. *Anal. Chem.* **2009**, *81*, 5111−5118.

(9) Cisse, I. I.; Kim, H.; Ha, T. *Nat. Struct. Mol. Biol.* **2012**, *19*, 623−627.

(10) (a) Reiner, J. E.; Crawford, A. M.; Kishore, R. B.; Goldner, L. S.; Helmerson, K.; Gilson, M. K. *Appl. Phys. Lett.* **2006**, *89*, 13903−13904. (b) Jofre, A.; Case, J.; Hicks, S. *Proc. SPIE* **2009**, *7400*, 740010−740014.

(11) (a) Gorris, H. H.; Rissin, D. M.; Walt, D. R. *Proc. Natl. Acad. Sci. U.S.A.* **2007**, *104*, 17680−17685. (b) Rissin, D. M.; Gorris, H. H.; Walt, D. R. *J. Am. Chem. Soc.* **2008**, *130*, 5349−5353. (c) Li, Z.; Hayman, R. B.; Walt, D. R. *J. Am. Chem. Soc.* **2008**, *130*, 12622−12623. (d) Rissin, D. M.; Kan, C. W.; Campbell, T. G.; Howes, S. C.; Fournier, D. R.; Song, L.; Piech, T.; Patel, P. P.; Chang, L.; Rivnak, A. J.; Ferrell, E. P.; Randall, J. D.; Provuncher, G. K.; Walt, D. R.; Duffy, D. C. *Nat. Biotechnol.* **2010**, *28*, 595−599.

(12) (a) Sims, P. A.; Greenleaf, W. J.; Duan, H.; Xie, X. S. *Nat. Methods* **2011**, *8*, 575−580. (b) Rondelez, Y.; Tresset, G.; Tabata, K. V.; Arata, H.; Fujita, H.; Takeuchi, S.; Noji, H. *Nat. Biotechnol.* **2005**, *23*, 361−365.

(13) Cohen, A. E.; Fields, A. P.; Hou, J. H.; Leslie, S. R.; Shon, M. J. *Isr. J. Chem.* **2009**, *49*, 275−282.

(14) Kapanidis, A. N.; Laurence, T. A.; Lee, N. K.; Margeat, E.; Kong, X.; Weiss, S. *Acc. Chem. Res.* **2005**, *38*, 523−533.

(15) Roy, R.; Hohng, S.; Ha, T. *Nat. Methods* **2008**, *5*, 507−516.

(16) (a) Schwille, P.; Meyer-Almes, F. J.; Rigler, R. *Biophys. J.* **1997**, *72*, 1878−1886. (b) Bacia, K.; Schwille, P. *Nat. Protocols* **2007**, *2*, 2842−2856.

(17) (a) This prediction was made with the DINAMelt Web Server at http://mfold.rna.albany.edu/?q=DINAMelt. (b) Markham, N. R.; Zuker, M. *Nucleic Acids Res.* **2005**, *33*, W577−W581.

(18) Levene, M. J.; Korlach, J.; Turner, S. W.; Foquet, M.; Craighead, H. G.; Webb, W. W. *Science* **2003**, *299*, 682−686.